Monitoring the rainfall intensity at two active volcanoes in Indonesia and Japan by small-compact X-band radars

Monitoring the rainfall intensity at two active volcanoes in Indonesia and Japan by small-compact X-band radars

Magfira Syarifuddin[1], Ratih Indri Hapsari[2], Djoko Legono[3], Satoru Oishi[4], Hanggar Ganara Mawanda[4], Nurnaning Aisyah[5], Makoto Shimomura[6], Haruhisa Nakamichi[6], and Masato Iguchi[6]

[1] Department of Dryland Farming Management, State Agriculture Polytechnic of Kupang, 85228, Indonesia
[2] Department of Civil Engineering, State Polytechnic of Malang, Malang, 65141, Indonesia
[3] Department of Civil and Environment al Engineering, Gadjah Mada University, Yogyakarta, 1234, Indonesia
[4] Graduate School of Engineering, Kobe University, Kobe, 657-8501, Japan
[5] Center for Volcanology and Geological Hazard Mitigation, Yogyakarta, 55166, Indonesia
[6] Disaster Prevention Research Institute, Kyoto University, Sakurajima, 891-1419, Japan

E-mail: magfira.syarifuddin@staff.politanikoe.ac.id

Abstract. Since 2015, collaborative research conducted by Indonesian and Japan scientists has initiated the installation of small X-band Multi-Parameter (X-MP) radars to mitigate the occurrence of rainfall-induced lahar in three active volcanoes in Indonesia and Japan: Merapi, Sinabung, and Sakurajima. This paper discusses the technical aspects of data acquisition, processing, and performance of the X-MP radar at the Merapi and Sakurajima volcanoes by comparing the estimated rainfall intensity acquired by the radar to three empirical radar-rainfall algorithms. The algorithms are based on radar reflectivity factor (Z_{HH}), specific differential phase shift (K_{DP}), and differential reflectivity (Z_{DR}). A new method of Constant Altitude Plan Position Indicator (CAPPI) interpolation by linear regression is also proposed for a more efficient computation. The first algorithm by Marshall-Palmer, which relies on Z_{HH}, gave the lowest average and maximum rainfall values compared with the other algorithms for all rainfall event cases. On the other hand, the other two algorithms, which involve the MP of radar by Bringi and Chandrasekar and Park *et al.*, gave closer rainfall intensity values with the estimated rainfall intensity acquired by the X-MP radar. These three rain rates give a closer temporal fluctuation when they are compared to the rain gauge-based rainfall intensity.

Keywords: X-band radar, dual polarimetry, rainfall intensity estimate, CAPPI interpolation.

1. Introduction

One of the deadliest hazards in volcanic regions is rainfall-induced lahar. Lahar is an Indonesian word that describes rapidly flowing, highly concentrated, and poorly-sorted sediment-laden mixtures of water and debris from a volcano. As rainfall is one of the triggering agents of lahar, some studies have

highlighted the importance of higher spatial and temporal resolution rain data for higher precision in lahar risk monitoring and prediction [1], [2].

The challenging aspect of rainfall monitoring in volcanic areas lies in two main problems. First, lahar usually occurs in a small area (less than 1 km) and is inaccessible. Second, the rain gauge network for rainfall measurement usually covers the downstream area, while the initiation of lahar usually happens in the upstream area. For the Merapi volcano, lahar usually occurs at elevations higher than 1200 m above sea level (asl) [3]. For the Sakurajima volcano, it usually occurs at elevations of greater than 400 m asl [4].

In an attempt to solve the problem of the scarcity of rain gauges in volcanic areas, some studies have recognized the importance of a small compact X-band Multi Parameter (XMP) radar to monitor the rainfall conditions [1], [2], [5]. The main feature of this compact X-MP radar is its ability to detect precipitation intensity up to a 50 m resolution in a 360° direction at 6-second intervals. This feature enables the radar to study the structure of cumulonimbus clouds that cause concentrated torrential rain, as well as its movement and development. The measurement extends up to a ~50 km radius, with the observation interval being approximately less than a minute to 2 minutes and the distance resolution starting from 100 m. This radar transmits a 3-cm wavelength, which is one of the shortest wavelengths transmitted by a weather radar system and falls in the range of raindrop size.

Since 2015, Japan and Indonesian scientists have deployed an X-MP radar for detecting the ejected tephra from an eruption and monitoring rain for lahar awareness in both countries. Some of the studies have suggested the improvement of X-MP radar sensitivity during some extreme rainfall events due to the uncertainty of the quantitative precipitation estimate (QPE) when compared with ground-based data [2], [5], [6]. A study by Putra *et al*. (2019) showed the ability of X-MP radar at Mount Merapi to cover up to 79% of the hourly rainfall, which is better than the satellite rainfall [6]. Although the previous studies are in agreement about the potency of this radar for remote monitoring of rainfall and its further application in hydrology, the algorithms used by the X-MP radar to estimate the rain intensity are unknown. Hence, it raises questions about the reliability of the estimated rain. Considering this problem, knowledge in radar data handling and processing is important for improving the accuracy of QPE and its application in disaster-related studies.

This paper discusses some technical aspects on the deployment of X-MP radar – the data acquisition and processing – and gives a conclusion about its performance to monitor rainfall conditions at two of the most active volcanoes in the world, Mt. Sakurajima and Mt. Merapi. This is expected to give an understanding of how to handle X-MP radar data and to visualize it for further advanced applications such as hydrological models.

2. Material and Methods

2.1. Study area and utilized data

The small compact X-MP radar at Mt. Merapi (Merapi X-MP) has been installed and operated since 2015 at the coordinate of 7.72 °S and 110.42 °E or approximately 7.6 km from the summit of Mt. Merapi. At its location at 742 m asl, the radar runs in a plan position indicator (PPI) scan-mode with a 150 m mesh resolution and a 2-minute time interval for each scan. It has 9 different elevation angles: 3°, 5°, 7°, 9°, 11°, 13°, 15°, 18°, and 21°. The resolution at 150 m mesh causes the highest elevation peak to exceed 18000 m AMSL at 50 km distance. Figure 1 shows the location of the radar, the area scanned by the radar, the height range of the PPI scan mode, and some observational stations and installed volcano instruments of the network around Mt. Merapi. Only three of the uppermost elevation angles – 15°, 18°, and 21° – are clear from the ground clutter caused by Mt. Merapi's topography (Figure 1).

The X-MP radar installed at Kagoshima (31.44 °N, 130.51 °E) is aimed to monitor the area of Mt. Sakurajima in Kagoshima Bay with the sectoral PPI scan mode. The Sakurajima X-MP operates at 2°, 5°, 10°, 15°, 20°, 25°, and 30° angular elevation levels. All of them are free from ground clutter created by the topography, as the lowest elevation angle at 2° exceeds 4 km asl at the peak of Mt. Sakurajima.

The spatial resolution is 100 m mesh and the temporal resolution is 1-minute. Figure 2 shows the location and the area scanned by the X-MP radar in Kagoshima.

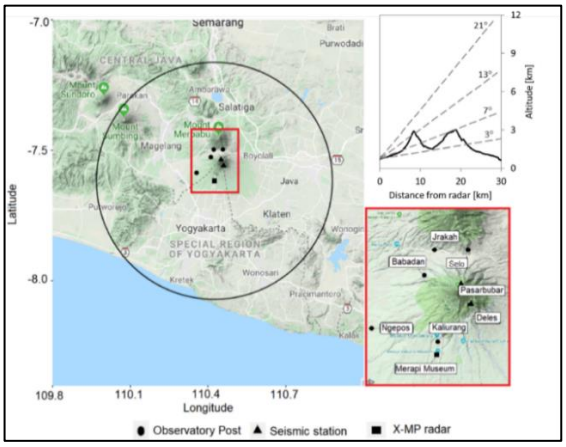

Figure 1. PPI scan mode of the coverage area monitored by the X-MP radar (left), some of the angular elevation of PPI and its equal altitude relative to the height of Mt. Merapi (top right), and zoomed-in area showing some installed instruments and the observatory posts at Mt. Merapi (bottom right).

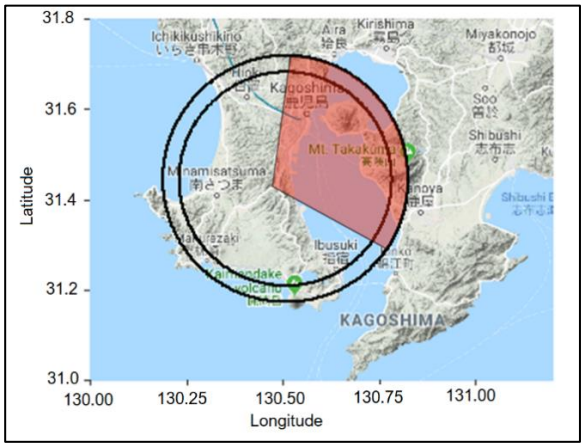

Figure 2. The sectoral PPI scan mode of Sakurajima X-MP radar, presented by the area shaded in red. The inner circle shows the delineated area scanned by the highest elevation angle, and the outer circle indicates the furthest area scanned by the lowest elevation angle.

2.2. X-MP radar description

The X-MP radar is a kind of polarimetry radar (polar: polarisation, metric: measure) that measures the polarization state of an electromagnetic field. The polarization information contained in the waves backscattered from a given medium is highly related to its geometrical structure reflectivity, size, shape, and orientation [7]. It transmits and receives in both horizontal and vertical polarization. In this study, the utilized X-MP radar is manufactured by Furuno Electric Co., Ltd from the WR-200 type.

The dual polarimetry radar measures reflectivity factor (Z), velocity (v), and spectrum width (W), similar to conventional radar, and other parameters as the result of the horizontal and vertical propagation. These are the parameters measured by X-MP radars:

1) Reflectivity factor, which is the efficiency of a target to reflect (absorb and re-radiate) radar energy. The horizontal propagation of reflectivity factor (Z_H) is mainly used to estimate rainfall intensity, R by a power law Z_H-R function.
2) Doppler velocity (v), which is described as the component of wind velocity parallel to the direction of the radar beam, either toward or away from the radar. The Doppler velocity is positive (+) when moving away from the radar (outbound), and negative (-) when moving toward the radar (inbound).
3) Doppler spectrum width (W), which is defined as the power weighted velocity distribution within the radar resolution volume.
4) Differential reflectivity (Z_{DR}), which is estimated as the ratio of the horizontal reflectivity (Z_H) over the vertical reflectivity (Z_V). Depending on the type of radar and its wavelength, certain ranges and threshold can be used to classify a meteorological object [7].
5) Specific differential phase shift (K_{DP}), which indicates the difference between propagation constants for horizontally- and vertically-polarized radar pulses over a given range.
6) Differential phase (Φ_{DP}), which is a measurement of the phase difference between *HH* (horizontally-transmitted and received) and *VV* (vertically-transmitted and received) co-polar echo. This parameter is not affected by partial beam blockage, attenuation, or radar miscalibration, which makes it useful for attenuation correction and QPE [8].

7) Copolar correlation coefficient (ρ_{HV}), which is defined as the zero lag correlation coefficient between horizontally- (*HH*) and vertically- (*VV*) transmitted and received copular signals. It shows the uniformity of the features being observed by the radar. The value ranges from 0 to 1.0, where a low ρ_{HV} (< 0.80), which implies low consistency between *H* and *V*, is more likely to be non-meteorological, such as birds or insects. Rainfall has a uniform shape, which leads to the value having a range from 0.95-1.0 [9]

Having information about these multi-parameters gives the benefits of improving the accuracy of precipitation estimates; being able to discern between heavy rain, hail, snow, and sleet; improving detection of non-meteorological echoes (such as ground clutter, chaff, anomalous propagation, birds, and tornado debris); and identifying the melting layer (such as bright band) [7], [8].

The X-MP radars used in this study measure all of the previously mentioned parameters and also gives a rain rate estimation every 2 minutes for the Merapi X-MP and 1 minute for Sakurajima X-MP. More detailed information for the radar specifications has been mentioned in a previous study [2].

2.3. Radar Data Processing and Radar-Rain Algorithms

Each scan of the X-MP radar data is stored in binary format with the *.scn extension. Using some scripts written in C language combined with the R Language, the data are converted into the Network Common Data Form (NetCDF) or Comma Separated Value (CSV) files. Radar data processing consists of three main procedural steps: 1) Data clean-up and storage, 2) QPE analysis, and 3) CAPPI interpolation and visualization. All of these steps are performed in the R Language of RStudio [10].

2.4. Radar data clean-up

Attenuation and ground clutter removal are the two performed processes for cleaning up the data from unwanted noise. The attenuation of radar is a common problem that is attributable to the radar's wavelength. A shorter-wavelength radar (X-band) is attenuated to a greater extent than a longer-wavelength radar (C-band). This problem causes a rainfall echo behind a stronger rainfall, which results in the reflection of a weaker electromagnetic wave, resulting in the under-estimation of rainfall intensity. This study uses the attenuation correction method proposed by Bringi and Chandrasekar (2001) [8]:

$$10\log Z_{HH}(r) = 10\log Z_{HH}' + \alpha\,[\Phi_{DP}(r) - \Phi_{DP}(0)] \quad (1)$$

$$10\log Z_{DR}(r) = 10\log Z_{DR}' + \beta\,[\Phi_{DP}(r) - \Phi_{DP}(0)] \quad (2)$$

where Φ_{DP} is the differential phase, Z_{HH} is the corrected reflectivity factor, Z_{HH}' is the attenuated reflectivity factor, Z_{DR} is the corrected reflectivity factor, and Z_{DR}' is the attenuated reflectivity factor calculated by the difference of differential phase of the system Φ_{DP} (0) and Φ_{DP} at distance *(r).*

Ground clutter in weather radar observations causes degradation of data quality and can lead to misinterpretation of radar echoes. In this study, all data that have ρ_{HV} lower than 0.9 and *v* equal to 0 were removed.

2.5. Radar rain estimation

Although the X-MP radar provides the rain rate information, it is unclear how the values were generated. This study calculates the rain rate using the three methods given in Table 1 for the rain events that occurred on Jan. 28, 2018 and Jan. 31, 2018 at Mt. Merapi and Jul. 7, 2018 at Mt. Sakurajima.

2.6. CAPPI interpolation

CAPPI interpolation was performed by selecting approximately 20% of data for each X-MP radar to model the bilinear interpolation rainfall according to time, coordinates, and altitude. Only five layers of the lowest elevation angle for each of the scan time were selected by assuming that a higher elevation angular angle has a higher chance to exceed the melting layer at an average of 5 km asl and contains other meteorological objects such as hail and stones.

The 3D interpolation model is done by time step-wise bilinear interpolation included in the *simecol* library of Rstudio. CAPPI interpolation is the most consuming process in radar data management [11]. Hence, to bypass the process, a linear regression model was developed between the interpolated 3D and

the PPI scan. Single or multiple dependent PPI scan data were used to fit the rainfall intensity at constant altitudes ranging from 1000 to 5000 m, every 50 m. The best fitted model was chosen based on the highest R^2 and model simplicity.

Table 1. Rain-radar equations and the condition to estimate rainfall intensity.

Methods	Condition	Equations	
Park *et al.* [9]	$K_{DP} \leq 0.3°$ km^{-1}	$R(Z_{HH}) = c_1 {Z_{HH}}^{a_1}$	(3)
	$K_{DP} > 0.3°$ km^{-1}	$R(K_{DP}) = c_2 {K_{DP}}^{b_1}$	(4)
Bringi and Chandrasekar [8]	$Z_{DR} > 0.5$ and $K_{DP} \leq 0.3°$ km^{-1}	$R(Z_{HH}, Z_{DR}) = c_3 {Z_{HH}}^{a_2} {Z_{DR}}^{b_2}$	(5)
	$K_{DP} > 0.3°$ km^{-1}	$R(K_{DP}) = c_4 \left(\frac{K_{DP}}{f}\right)^{b_3}$	
Marshall-Palmer [10]	-	$R(Z_{HH}) = \left(\frac{Z_{HH}}{200}\right)^{a_4}$	(6)

Notes: a, b, and c are constants: a_1 = 0.819, a_2 =1.07, a_4 = 0.625, b_1 = 0.823, b_2 = -5.97, b_3 = 0.85, c_1 = 7.07 x 10^{-3}, c_2 = 19.63, c_3 = 3.93 x 10^{-3}, and c_4= 129; f is radar frequency in GHz, equal to 9.47.

3. Results and Discussion

3.1. Ground clutter removal and attenuation correction

An example of the horizontal radar reflectivity factor (Z_{HH}) before and after the ground clutter removal and attenuation correction for the Merapi X-MP is presented in Figures 3. The ground clutter removal is an important aspect for the Merapi X-MP as it removes all the area blocked by Mt. Merapi. The radar already receives weaker rain signals due to the blockage of the 7 lowest elevation angles (Figure 2). Removing the clutter also clears some of the radar reflectivity at the eastern flank of the mountain (Figure 3). The attenuation correction also reduces some of the unmeasured area indicated by the red circles in Figure 3.

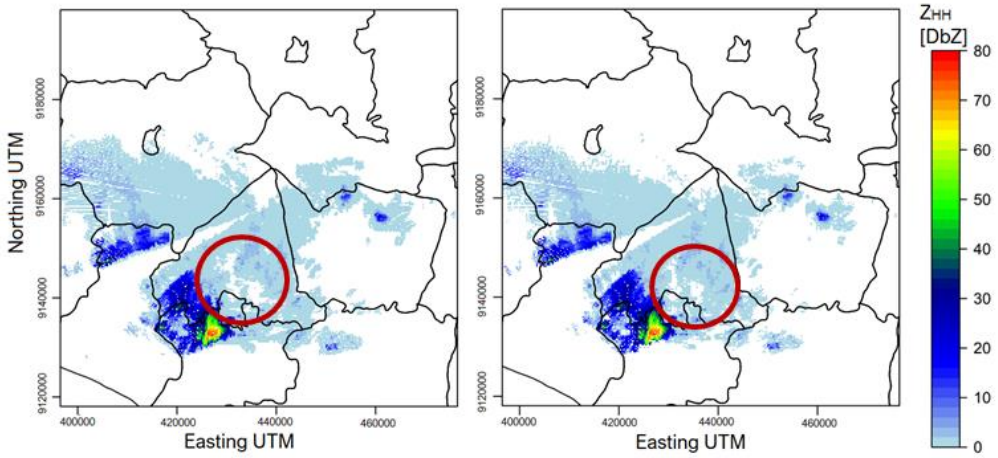

Figure 3. An example of radar reflectivity before data clean-up (left) and after data clean-up (right) for the rain event that occurred on Jan. 31, 2018 at 16:58 UTC.

3.2. CAPPI interpolation

The best fitted model is given by angular elevation 5° for Merapi X-MP and 2° for Sakurajima X-MP with R^2 = 0.81 and R^2 = 0.67, respectively. The linear regression model fitted the CAPPI interpolation

for the radar at Mt. Merapi better than the radar at Mt. Sakurajima. This was caused by the limitation of the altitude in the interpolation method. The rainfall was estimated only for the altitude ranging from 1000-5000 m asl. As the Sakurajima X-MP ran at sectoral PPI scan mode (Figure 2) and is located more than 10 km from the area of Mt. Sakurajima, it monitored the rain at elevations higher than 4 km asl above the Mt. Sakurajima area. Consequently, most of the rainfall monitored by this radar belongs to the altitude higher than the assumed melting ratio. These values were reduced significantly by the bilinear interpolation.

Figure 4 gives an example of a 2D CAPPI of Furuno rain rate estimate at an elevation of 1200 m asl for the X-MP radar compared with the rain map provided by radar at the same time at 1500 m asl for Mt. Merapi. The rain map provided by the X-MP radar program showed rain occurrence in the area that had been removed by the data cleaning. Further investigation is needed to find out the validity of the rain map, as this area may be strongly affected by the topography of Mt. Merapi.

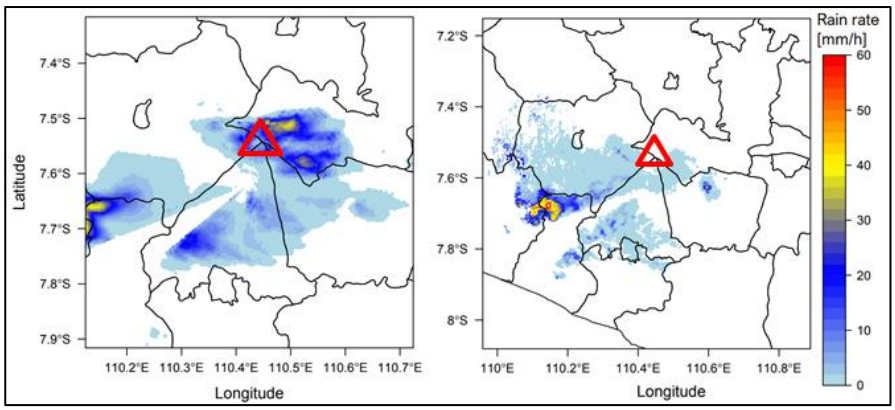

Figure 4. The CAPPI of the rain map (left) compared to the CAPPI interpolation at 16:40 UTC on Jan. 31, 2018. The CAPPI-interpolated rain map is at 1500 m asl. The position of Mt. Merapi is indicated by the red triangle.

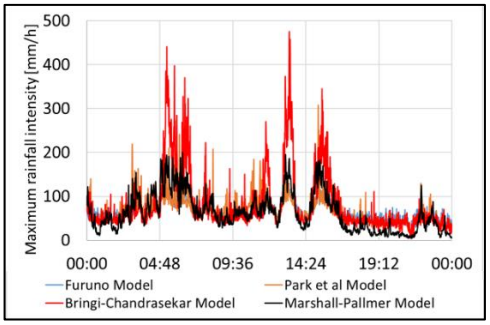

Figure 5. Temporal maximum rainfall intensity in Mt. Sakurajima on 2018, Jul. 7 local time.

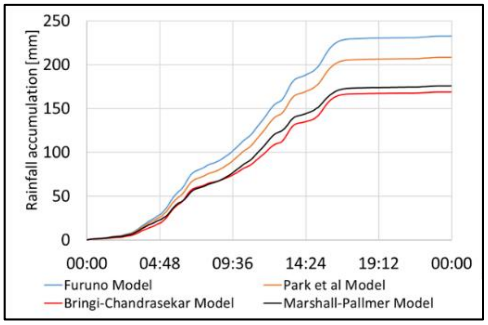

Figure 6. Accumulated rain depth [mm] in Mt. Sakurajima on 2018, Jul. 7 local time.

3.3. Rainfall intensity and rain depth

The maximum temporal rainfall intensity estimated from all the algorithms in Table 1 compared to the rainfall given by the original rainfall intensity of the X-MP radar at Mt. Sakurajima is presented in Figure 5, while Figure 6 shows the temporal areal rain depth at Mt. Sakurajima. The total rain depth received for the two selected cases at Mt. Merapi are presented in Figures 7 and 8.

Similar to the results at Mt. Sakurajima, the Marshall-Palmer algorithm (R3) gave the lowest rain rate compared to all of the other algorithms. The Furuno original rain rate, on the other hand, gave close results to the Park *et al*. model (R1). This shows that the algorithms used by Furuno for estimating the rain rate may be based on the same algorithms involving the K_{DP} and Z_{HH}. Although Bringi and

Chandrasekar's algorithm gave the highest rainfall intensity (Figure 5), however, on average, it has the lowest rain depth values in Sakurajima. This result may be affected by Z_{DR} values that increase the rainfall intensity at some specific areas only.

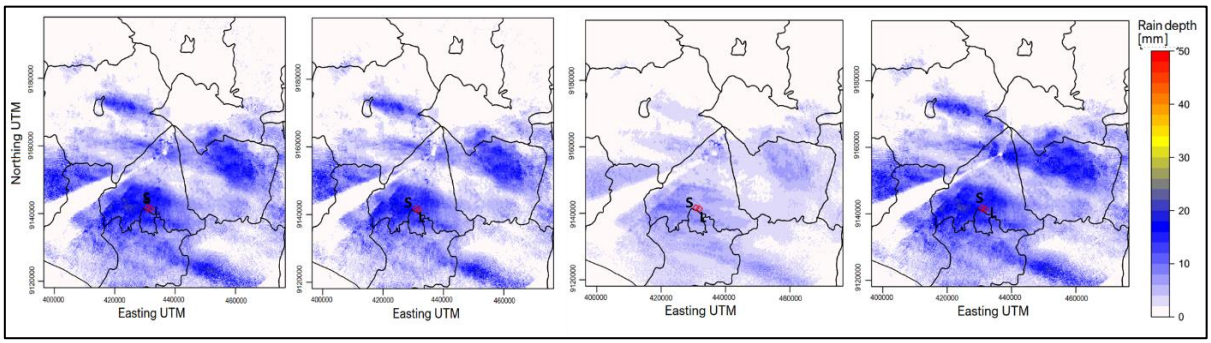

Figure 7. Rain depth estimated by X-MP radar at Mt. Merapi on Jan. 28, 2018. From the left panel: Park *et al*. (R1), Bringi and Chandrasekar (R2), Marshall and Palmer (R3), and Furuno. The Sipil rain gauge is indicated by the red point and the letter S.

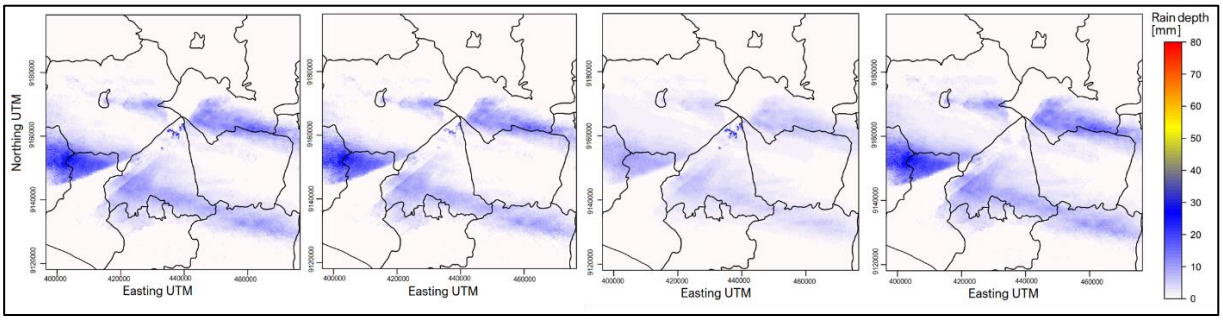

Figure 8. Rain depth estimated by X-MP radar at Mt. Merapi on Jan. 31, 2018. From the left panel: Park *et al*. (R1), Bringi and Chandrasekar (R2), Marshall and Palmer (R3), and Furuno.

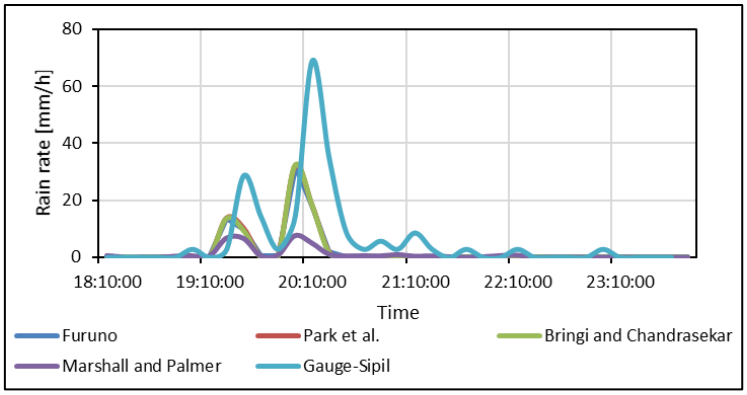

Figure 9. Point comparison between the radar rain estimate and ground-based rain rate measured by the Sipil gauge indicated in Figure 7 for the rainfall event on 2018, Jan. 28.

A temporal comparison of the 10-minute rain rate is presented in Figure 9. Although the radar rain rate was able to show similar temporal fluctuations, it still could not reach the maximum intensity that occurred at 20:20. The radar's rain rate also occurred earlier than the rain gauge measurement, which is reasonable as the CAPPI interpolation data were extracted from 1200 m asl, which causes a delay of 10 to 20 minutes. The lower rain rate intensity by the radar causes the correlation coefficient between radar rain and ground-based rain gauge to range from 0.53-0.59 for the selected cases at Mt. Merapi. These

issues have been addressed in a previous study [2], which encourages a better method to improve the radar-rain algorithm empirically or by further analysis of drop size distribution.

4. Conclusion

Two X-MP radars had been installed to monitor the rainfall at Mt. Sakurajima in Japan and Mt. Merapi in Indonesia. Both radars are dual-polarimetry radars that give multi-parameters, which is believed to improve the accuracy of QPE. Radar data handling started with ground clutter removal and attenuation correction. It is apparent that the rain map data provided by the X-MP radar at Mt. Merapi gives higher rain rates in the areas recognized to be strongly affected by ground clutter. Using a linear regression model, a more efficient technique can be applied for CAPPI data interpolation. The algorithm used by the radar company manufacturer is in agreement with the Park *et al*. model that relies on K_{DP}. Although the X-MP radar underestimated the rain rate, however, in general, the delay period and the temporal fluctuation is still consistent with the ground-based rainfall intensity.

References

[1] Marra F, Nikolopaulus EI, Creautin JD, and Borga M 2014 *J. Hydrol* 519 (B) pp 1607–1619.
[2] Syarifuddin M, Oishi S, Hapsari R, Legono D, and Iguchi M 2017 *Adv. Water. Resour*. 110 pp 249–262.
[3] Legowo D 1981 *J. Hydrol* 20 122–134.
[4] Takeshi, T *International Journal of Erosion Control Engineering* 4 (1)
[5] Hapsari R, Oishi S, Syarifuddin M. Asmara R, and Legono, D 2019 *J. Disaster Res.* 14(5) pp 811–828.
[6] Putra S, Ridwan B, Yamanoi K, Shimomura M, Sulistiyani, and Hadiyuwono D 2019 *J. Disaster Res.* 14(1) pp 80–89.
[7] Park SG, Bringi VN, Chandrasekar V, Maki M, and Iwanami K 2005 *J Atmos Ocean Tech* 22 pp 1621–1631.
[8] Bringi VN and Chandrasekar V 2001 *Polarimetric Doppler Weather Radar: Principles and Applications* (Cambridge University Press)
[9] Marshall, JS and Palmer WM 1948 *J.Meteor*. 5 pp 154–166.
[10] R Core Team 2017 R: A language and environment for statistical computing. *R Foundation for Statistical Computing*, Vienna, Austria. URL https://www.R-project.org/.
[11] Yang L, Jang BJ, Lim S, Kwon KC, Lee SH, and Kwon KR 2015 *Journal of Korea Multimedia Society* 18(4) pp 473–482.